Design optimization of a soft micro-robot for medical intervention

Alexandre Thuillier, Sébastien Krut, Nabil Zemiti, Philippe Poignet

Design optimization of a soft micro-robot for medical intervention

Alexandre Thuillier, Sebastien Krut, Nabil Zemiti, Philippe Poignet

***Abstract*— In this paper, a design method of a soft fluidic micro-robot (SMR) used for medical intervention in the context of cochlear implant insertion is proposed. Two centerlines are used: SMR's neutral axis and the helicoidally shaped pipe inside the cochlea called scala tympani (ST). The average distance between these two lines is defined as an objective function to be minimized. To achieve this, a cochlea implant has been hollowed-out to create an optimally shaped pneumatic chamber to be pressurized. The variation of the bending moment and second moment of area along the SMR's longitudinal axis have been employed to ensure that its curvature radius under pressure follows the ST's centerline. Finite element analysis is used to iterate over the parametric pneumatic chamber until the objective function is minimized.**

Simulated insertions have been conducted to test the optimal design and they shows that the proposed method may improve the insertion of straight wall electrode arrays by reducing the collisions with the anatomy. This is the first step toward the development of a closed loop active medical device for inner-ear intervention.

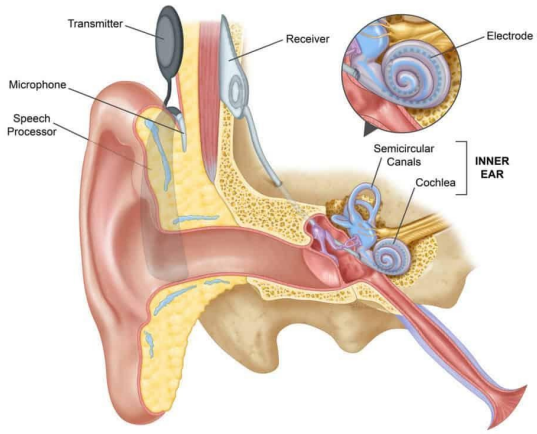

Fig. 1. Illustration of a cochlear implant within the inner-ear [10]

I. Introduction

Hearing loss is a disease that affects millions of adults worldwide. Idiopathic and noise are two causes of hearing loss affecting more than 40 millions adults in the U.S only that can be attempted to cure by either hearing aids, corticosteroids or cochlear implants (CI)[1]. This paper is focused on the latter.

CI is a solution that bypasses the natural mechanical anatomical chains, that transforms an acoustic wave into an electric stimulus, by electro-stimulating the Auditory Nerve (AN, Fig. 2) within the inner-ear directly. CI consists of a microphone sensing acoustic waves placed behind the auricle which is connected to a speech processor and a transmitter. This transmitter emits the transformed acoustic waves to an electric signal to a receiver placed in the bone behind the external ear called mastoid bone. The signal is then sent to the AN by the mean of the CI and will be interpreted as sound by the brain.

To proceed, the neuroprothesis needs to be surgically inserted into a helical shaped canal called scala tympani (ST) in the cochlea bone (Fig. 1 and 2). Being in the inner ear, the access to that canal is done by an opening in the mastoid bone, drilled down to the tympanic cavity that gives the surgeon two-choices to access the ST. Either by opening the round window membrane (RWM) or by cochleostomy (CO) as illustrated in Fig. 2. Usually, the whole process is done manually by the mean of tools. The best approach is decided during the mastoidectomy [3]. Once inserted, the CI stays in the ST.

The complexity of this procedure is that the cochlear implant insertion is performed blindly, with the surgeon relying only through force feedback. The close proximity of the breakdown and detection thresholds of the anatomy and the surgeon's sensory perception further complicates the process, increasing the risk of intra-cochlear traumas [4]. The risks of traumas associated with the insertion of a CI in the ST are from the elevation of the basilar membrane (BM) to the ST's perforation leading to a translocation into the scala vestibula (SV).

Due to the risks involved, this surgical procedure is typically reserved for patients with low or completely absent residual hearing, as the aforementioned traumas can lead to total hearing loss. However, this decision to exclude certain patients is problematic, considering that preserving residual hearing can contribute to faster hearing recovery in the future [9].

Fortunately, commercially available solutions already exists with two kinds of CI that can be distinguished:

- Straight lateral wall electrode array (LW) is naturally straight and frictions against the lateral wall of the ST. Buckling may happen due to insertion beyond resistance leading to the rupture of the BM in the very first ST turn and the same behavior may be observed when the CI is almost fully inserted with a jammed tip causing basal buckling that is not detectable by the surgeon in clinical pratice. These issues have been studied by manufacturers. Optimizing the tip design, downsizing the apical width and length are working solutions but the final behavior of the straight neuroprothesis will always have a random outcome [7].
- Pre-curved perimodiolar electrode array (PM) is naturally curved, forced straight with an embedded strand.

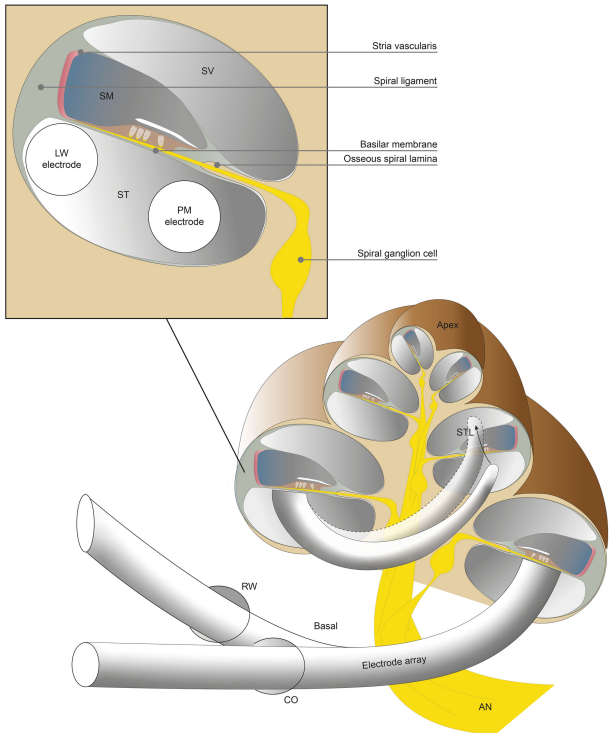

Fig. 2. Cross section of the cochlea with an implanted cochlear implant [2], RW: Round Window, CO: Cochleostomy, STL: Scalar Translocation, AN: Auditory Nerve, SM: Scala Media

There are two insertions techniques: standard insertion technique (SIT) and advanced of stylet technique (AOS). For SIT, the CI is inserted as a straight electrode array and then the strand is pulled out. For AOS, the CI is partially inserted in the ST, pushed inside while sliding on its inner strand. SIT leads to less force exerted against the BM in comparison to LW because they are shorter while PM with AOS have almost zero contact with the lateral and medial wall. However, pre-curved CI may not match the individual helicoidal shape which could lead to a large number of translocations [8].

Both cochlear implants are made with flexible materials and have a length superior to their cross-sectional dimensions. The electrodes and wires, made of an alloy, are embedded within the structure.

A. State of the Art

Several strategies are being used to solve the problem of cochlear implant insertion. Steerable electrode array by pulling an embedded strand in them has been studied [11]. The advantage of that actuator is the thin cross-section footprint of the strand within the CI. Magnetically guided active electrode arrays with a permanent magnet at their tip are a viable solution [12]. An external magnetic source moving outside the patient's head is required. Their results are interesting but the permanent magnet's removal from the CI's tip may leads to new trauma. Concentric tubes embedded into a straight CI is a feasible solution [13], simulation results show that a low trauma insertion is possible with

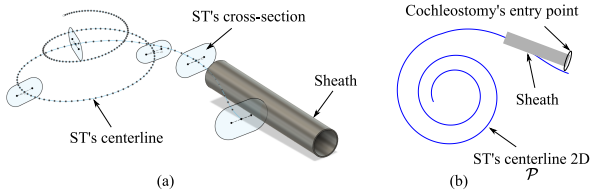

Fig. 3. Desired path considering cochleostomy insertion with 5 examples of the ST slot's shaped cross-section: (a) 3D model of the ST, (b) 2D model used for the study

this strategy. Active CI based on shape memory alloy has been seen as a potential solution [14], [15] even though the activation temperature should be carefully chosen to not cause damage to the ST epithelial cells or run into a thermal runaway therefore actuation uncertainty. Finally, fluidic actuator has been studied at scale 3:1 and shows promising results [16].

B. Our work

In this paper, the reader is expected to see a methodology to design and manufacture a fluidic robotized CI. We will (i) investigate on the upgrade of a straight wall cochlear implant by considering the geometry of the inner-ear from a model, (ii) ensure that the new cochlear implant permit a low-trauma insertion.

II. Methodology

A part of the cochlea implant's silicone-made bulk is hollowed to create a pneumatic chamber. Inflating this chamber will induce a bending moment which will curve the CI. This new hollowed structure is apparent to a pneumatic soft robot or a fluidic soft micro-actuator (SMA). Attention should now be focused on the pneumatic chamber's geometry. When pressurized, a changing curvature radius along the longitudinal axis of the robot is desired to satisfy a low trauma-insertion within the ST as depicted in Fig. 6.

The pneumatic cavity is designed to satisfy the final shape of the CI at full insertion then a proper insertion of the CI in the ST is checked *a posteriori*. A rigid sheath in the ST is used to constrain the SMA's proximal end (Fig. 3 (b)).

A. Objective

The objective is to find the optimal chamber geometry from an initial shape and actuator pressure to minimize the distance between the ST and the SMA centerlines.

Straight cochlear implant uses contact forces against the anatomy to bend, leading to a high magnitude of insertion forces which peaked after the first impact upon the basal turn [7]. Such contacts are expected to be reduced thanks to this SMA and shape optimization method.

B. Constraints

1) Anatomical: The SMA size shall be dictated by the ST geometry that varies greatly between individuals [18] so only average values will be considered knowing that patient-specific SMA can be designed.

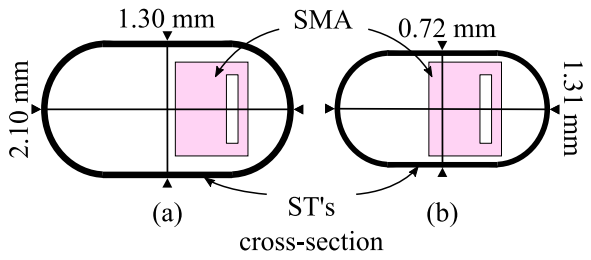

Fig. 4. ST and SMA cross-section (a) near the entry point (b) after 1 turn or 360°

As depicted in Fig. 2 and 3, insertion by cochleostomy is assumed with a diameter range between 0.8 and 2.0mm [19]. With this procedure, an entry point in the cochlea is aligned with the ST's centerline where few mm of sheath is inserted as a guide for the SMA [17].

Once inside the ST, its dimensions are 2.1mm wide for 1.30mm high at the beginning and 1.31mm wide for 0.72mm high after 1 turn where the distal tip desired position of the SMA shall be for a device this long as illustrated in Fig. 4 and Fig. 6. The logarithmically spiral shaped's path $\mathcal{P}$ to follow is generated by a phenomenological model of the scala tympani's centerline [20].

Finally, as the helicoidally shaped ST has an elevation of only ∼1mm after the first basal turn, a 2D study is considered as a proof of feasibility and shall be supported by a 3D study subsequently only if deeper insertion is needed but the CI electro-stimulation beyond the depth of 25 mm or 1 $^1/_4$ turn into the cochlea (Fig. 6) does not seem necessary [7], [18].

2) Geometry: The CI electro-stimulation beyond the radiological depth of 360° to 450° or 1 turn to 1 $^1/_4$ turn into the cochlea (Fig. 6) does not seem necessary [7], [18]. Thus, the current trend for newly developed CI is a length converging towards 20 mm to 25 mm for the best balance between cochlea trauma and performance. The smallest distal height is approximately 0.4 mm and the biggest 0.5 mm while the basal diameter ranges between 0.6 and 1.3 mm [7], [21].

Fig. 5 depicts the device of a length l = 22 mm, height of h = 0.5 mm and a constant width of b = 0.7 mm. This constant width will be changed in the future as discussed in Section IV. Since the length l and width w of this SMA are based on a commercially available cochlear's implant, it is important to fix those parameters as constant.

The cochlea's bone being similar to a logarithmic spiral, a different curvature radius is needed along its longitudinal axis. This desired bending might be achieved with a pneumatic chamber shaped as a thin 3D trapezoid. With a trapezoidal shape for the pneumatic chamber: further toward the distal tip, the smaller is the desired radius of the CI and smaller is the second moment of area thus smaller is the curvature radius of the CI (Fig. 5 (a)). The opposite is also true.

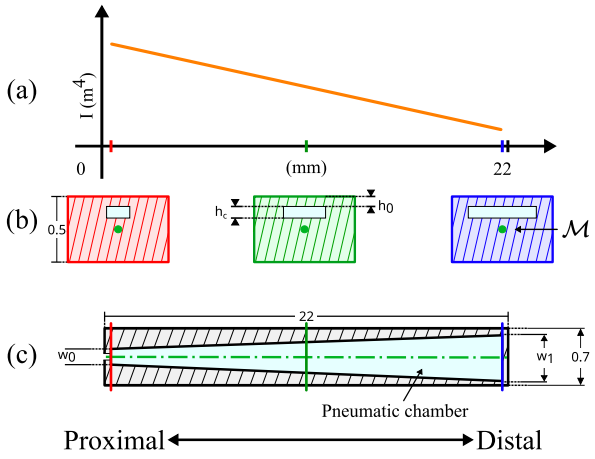

Fig. 5. (a) Second moment of area along the longitudinal axis, (b) cross-section at the proximal, middle and distal position, (c) SMA top view with the trapezoidal pneumatic chamber in cyan

C. Simple objective optimization problem

For the sake of simplicity, the design variables are h_0, w_0, w_1 and P respectively the top layer membrane height, the distal and proximal width of the pneumatic chamber and the input pressure (Fig. 5 (b, c)), with $w_0 < w_1$ and $(w_0, w_1) \in [0.1, 0.4]$ mm. No constraints has been defined for the pressure.

The desired path and the SMA's neutral axis are respectively depicted as $\mathcal{P}$ and $\mathcal{M}$ in Fig. 6.

$\mathcal{M}$ is discretized in n samples. For each sample $\mathcal{M}_i$, with $i \in [1, n]$, the shortest distance from $\mathcal{M}_i$ to $\mathcal{P}$ is computed. It is important to note that a radiographic positioning method is employed (Fig. 6). An axis is drawn from the cochlea's center to the starting point of the Cochlear's Hook noted θ_0 and an angle θ can be measured from this axis to any axes crossing $\mathcal{P}$ and the cochlea's center. In some cases, as shown in Fig. 6, the SMA bending is so important that the shortest distance from $\mathcal{M}_i$ to $\mathcal{P}$ is wrong so the shortest distance must be found in the given interval $\theta^* \in [\theta_{min}, \theta_{max}]$, which is defined empirically for each i. Therefore, $\mathcal{P}_i(\theta^*)$ can be noted as the radiologically positioned closest point on $\mathcal{P}$ from $\mathcal{M}_i$.

Using (1), the RMSE Ψ between the SMA and ST centerlines is then computed and used in the optimization workflow.

$$\begin{aligned} &\min_{w_0, w_1, h_0, P} \Psi = \sqrt{\frac{\sum_{i=1}^{n} ||\mathcal{P}(\theta^*) - \mathcal{M}(i)||^2}{n}} \\ &\text{subject to : } \theta^* = \underset{\theta \in [\theta_{min}, \theta_{max}]}{\arg\min} ||\mathcal{P}(\theta) - \mathcal{M}(i)|| \end{aligned} \tag{1}$$

With l the total length of the SMA, n the total number of samples of the SMA's neutral axis. $[\theta_{min}, \theta_{max}]$ is an arc on the path $\mathcal{P}$ where θ^* must be found, θ^* is the radiological position of the closest point between $\mathcal{M}(i)$ and the path $\mathcal{P}$ (Fig. 6).

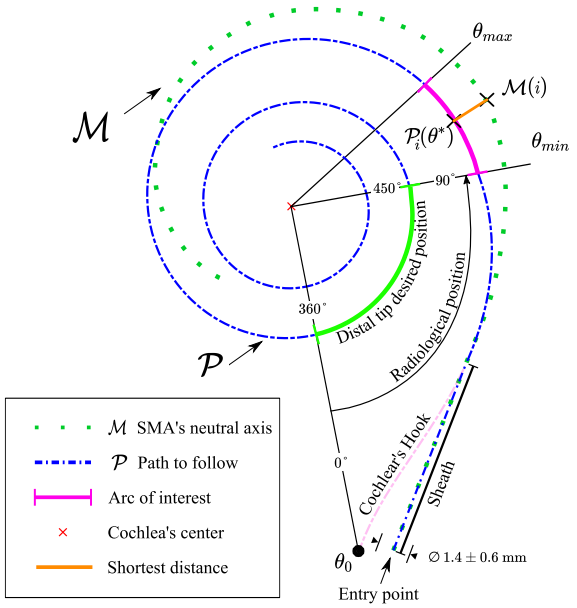

Fig. 6. Illustration of the optimization processus. Here the SMA is under pressure and its neutral axis $\mathcal{P}$ is far from the desired spiral shape $\mathcal{M}$

D. Finite Element Analysis

1) Setup: A static structural analysis study with large deflection has been set in Ansys©. The parametric CAD is generated with DesignModeler©. Three probes with $n = 50$ regularly distributed sampling points were placed within the meshed SMA from the proximal to the distal end at the centerline $\mathcal{P}$, top and bottom surfaces. These two lasts probes are used in Section IV to visual the ballooning effect that occurs with pneumatic actuator. Mesh was rendered with coarsed TET10 to improve convergence.

Finally, to simulate the sheath, a surface has been extracted from the SMA's bottom surfaces. In this dedicated surface, normal displacements were set to 0. Consequently, displacement's constraints between the SMA and sheath are considered without contacts hence no heavy computation. An analysis with a meshed sheath will be done in the future.

2) Material: The material used in this study was the EcoFlex 00-30 by Smooth On. Being hyperelastic, the 3rd order Yeoh model was used in the simulation to describe the material non-linearity [5].

C_1	C_2	C_3	
1.00×10^{-1}	1.20×10^{-2}	4.96×10^{-5}	MPa

TABLE I

CONSTITUTIVE MODEL PARAMETERS OF ECOFLEX 00-30

3) Workflow: The workflow is pictured in Fig. 7. Initially, in step (a), design parameters are set to $w_0 = 0.1$ mm, $w_1 = 0.4$ mm, $h_0 = 0.03$ mm and $P = 0.08$ MPa. In steps (b, c), the structure is generated, meshed and a solution is found taking into account boundaries conditions set in II-D.1. Then, the objective function detailed in Eq. 1 is solved. If the current set of parameters minimizes the distance error between the SMA and ST centerlines then verification and validation are performed in step (g). Otherwise, the algorithm iterates.

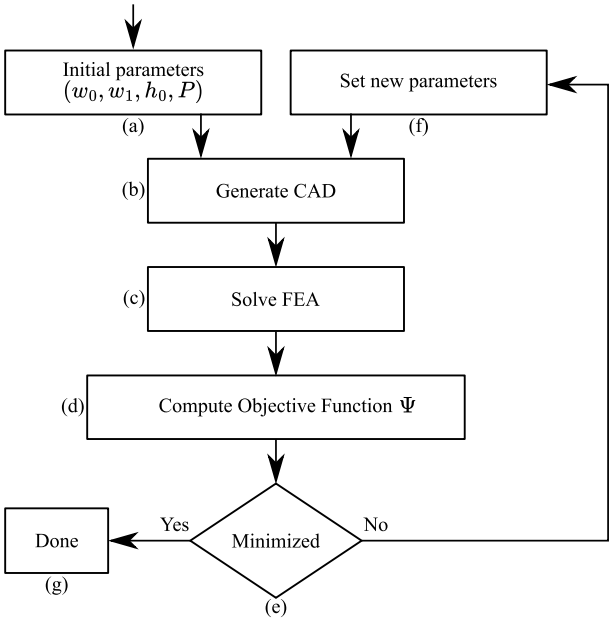

Fig. 7. Flow chart of the optimization process

4) Verification: Values in Table II are obtained from the previously described algorithm and they comply with the design requirements.

w_0	w_1	h_0	P
0.234	0.4	0.1	0.128
mm			MPa

TABLE II

DESIGN VARIABLES RESULT FOR THE SMA'S OPTIMAL BENDING

A collision analysis at the final position was then done to verify if contacts between the SMA and anatomical wall exist (Fig. 8). A strictly visual observation shows that the collisions are acceptable for now but an investigation should be conducted to estimate the contact forces between the SMA and the cochlea in order to estimate the possible trauma.

5) Validation: Finally, a complete insertion is simulated as illustrated in Fig. 10 to validate the optimal geometry. A new variable $l_i \in [0, l]$ defines the state of the insertion in the cochlea with $l_i = l$ being a complete insertion of the CI in the ST. To proceed, a new set of design variable is set with only the pressure P to be optimized. The optimal pressure P^* for each step in the insertion was obtained by using the same workflow depicted in Fig. 7 with the new set of design variables.

While Fig. 10 illustrates the insertions, Fig. 9 shows the expected actuator's pressure profile to follow depending on

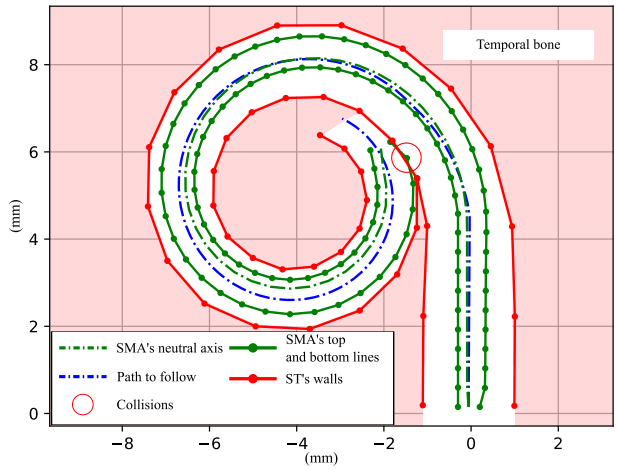

Fig. 8. Simulation results: SMA's final position at full insertion. The redish background illustrate the bone hence for the forbidden zone. A ballooning effect can be observed thanks to the topline

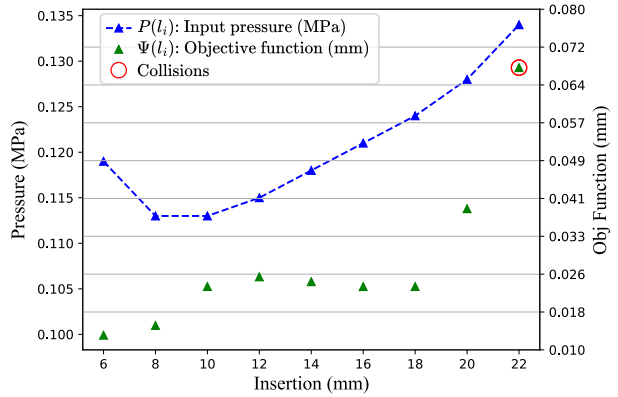

Fig. 9. Simulation results: pressure profile during a full insertion, $l_i \in [6, 22]$ (mm)

the insertion with the optimal SMA's geometry generated previously in Section II-D.4.

III. Simulation Results

The completed insertion shown in Fig. 9 and 10 can be visually examined. In red, the simplified anatomical walls of the ST acting as a physical limit which should not be trespassed or traumas may occur. The SMA's top, center and bottom line are illustrated in green while the ST's centerline is in blue. Collisions are circled but not taken into account during the FEA step (Fig. 7 (c)). From these simulation results, it is expected to have a collision on $l_i = 22$ mm at full insertion. This contact and the trauma associated should be identified as explain is Section I in future work. The initial pressure peak at insertion $l_i = 6$ mm is from unknown reason. But, these preliminary results show that a minimally traumatic insertion may be achieved with an optimally designed SMA.

IV. Discussion

Two important points should be noted : (i) the SMA is subject to balloon effect, when under pressure the silicone will have a high radial stretch. Attention should be paid that this ballooning effect may be underestimate in the simulation and more collisions are expected in the future experiments. (ii) Looking at the robot's proximal position in Fig. 8, it is clear that the current proximal position and orientation of the SMA are not optimal. Therefore, we can retrospectively assume that the intermediate insertions can be optimized by moving that proximal pose. These motions are not trivial and should be carefully studied and related to the SMA's actuation pressure. Nevertheless, these preliminary results are promising to reduce the intercochlear damage that may occurs during a CI insertion.

To get more realistic results, it is important to manufacture the SMA and insert it into a 1:1 scale cochlea so the traumas can be measured with a force sensor and compared with the average force profile of classic and state-of-art cochlear implants.

Modification of the CI initial hypothesis should be addressed for future studies :

- The SMA geometry have been simplified. Starting with the overall SMA dimensions: a tapered shape should be considered since CI are normally wider at the base than at the tip.
- It has been said earlier that the current position and orientation of the sheath might not be optimal. Therefore, an investigation should be performed taking into account the anatomical constraint of the middle-ear. This future work might guide us toward a new optimal path that will probably not be the exact centerline of the ST as used herein.

Finally, by having established a design method to manufacture an optimal SMA for a given path in the cochlea, this device could be used to deliver drug into the cochlea. Such a system will allow us to integrate embedded sensors, improve echogenicity with specific materials, complexify the geometry of the pneumatic chamber and close the loop for a future control.

V. Conclusion

In this paper, a shape optimization based on finite element analysis for a soft fluidic micro-actuator has been presented. This method has been conceived for a controlled insertion of an intrinsically-actuated robotized cochlear implant in the cochlea. An optimal geometry of the inner CI's pneumatic chamber has been generated and tested in a simulated cochlear implant insertion. A visual observation of the collision between the anatomy wall and the robot shows a possible low trauma insertion. Future works should take into account different materials for the SMA, variability in the cochlea anatomy and an optimal insertion angle.

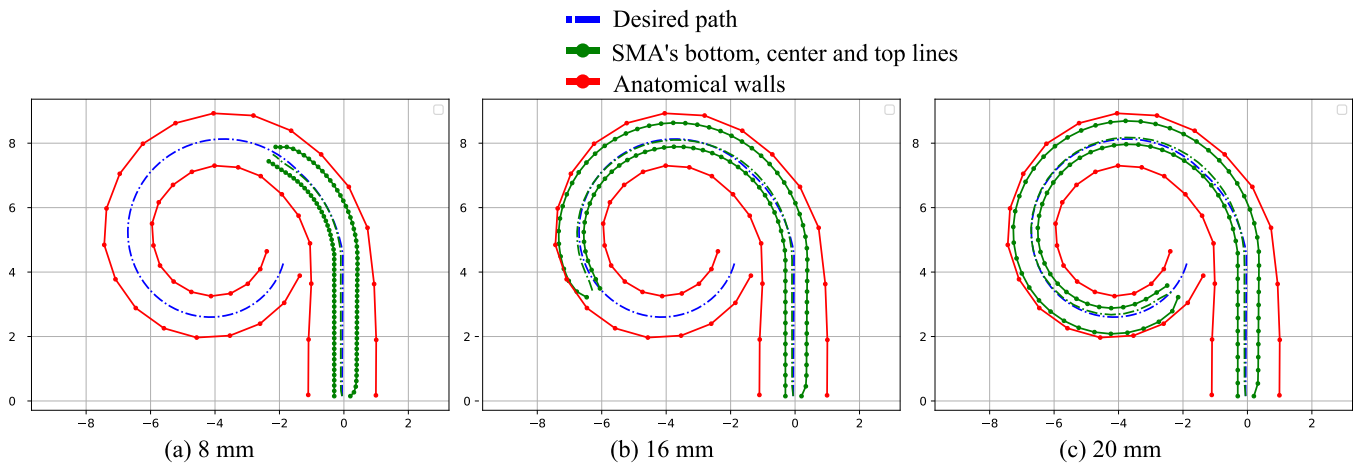

(a) 8 mm (b) 16 mm (c) 20 mm

Fig. 10. Simulation results: insertion at (a) $l_i = 8$ mm, (b) $l_i = 16$ mm, (c) $l_i = 20$ mm. A ballooning effect is observed at every steps.

REFERENCES

[1] Marcello Peppi, A. Marie, Aurore Marie, C. Belline, and Jeffrey T. Borenstein, 'Intracochlear drug delivery systems: a novel approach whose time has come', Expert Opinion on Drug Delivery, 2018.

[2] S. Jwair, H. Versnel, R. J. Stokroos, and H. G. X. M. Thomeer, "The effect of the surgical approach and cochlear implant electrode on the structural integrity of the cochlea in human temporal bones," Scientific Reports, vol. 12, no. 1. Springer Science and Business Media LLC, Oct. 12, 2022. doi: 10.1038/s41598-022-21399-7.

[3] G. J. Basura, O. F. Adunka, and C. A. Buchman, 'Scala tympani cochleostomy for cochlear implantation', Oper. Tech. Otolayngol. Head Neck Surg., vol. 21, no. 4, pp. 218–222, Dec. 2010.

[4] D. De Seta et al., 'Damage to inner ear structure during cochlear implantation: Correlation between insertion force and radio-histological findings in temporal bone specimens', Hear. Res., vol. 344, pp. 90–97, Feb. 2017.

[5] L. Marechal, P. Balland, L. Lindenroth, F. Petrou, C. Kontovounisios, and F. Bello, "Toward a Common Framework and Database of Materials for Soft Robotics," Soft Robotics, vol. 8, no. 3. Mary Ann Liebert Inc, pp. 284–297, Jun. 01, 2021. doi: 10.1089/soro.2019.0115.

[6] A. A. Eshraghi, N. W. Yang, and T. J. Balkany, 'Comparative study of cochlear damage with three perimodiolar electrode designs', Laryngoscope, vol. 113, no. 3, pp. 415–419, 2003.

[7] F. Risi, 'Considerations and rationale for cochlear implant electrode design-past, present and future', J. Int. Adv. Otol., vol. 14, no. 3, pp. 382-391, 2018.

[8] A. Dhanasingh and C. Jolly, 'An overview of cochlear implant electrode array designs', Hear. Res., vol. 356, pp. 93–103, 2017.

[9] G. P. Rajan, G. Kontorinis, and J. Kuthubutheen, 'The effects of insertion speed on inner ear function during cochlear implantation: A comparison study', Audiol. Neurotol., vol. 18, no. 1, pp. 17–22, 2012.

[10] "About Cochlear Implants" Children's Hospital & Medical Center. Accessed: Feb. 28, 2023. [Online]. Available: https://www.childrensomaha.org/department/ear-nose-throat/cochlear-implant-program/about-cochlear-implants/

[11] J. Zhang and N. Simaan, 'Design of underactuated steerable electrode arrays for optimal insertions', J. Mech. Robot., vol. 5, no. 1, p. 011008, Feb. 2013.

[12] C. M. Hendricks et al., 'Magnetic steering of robotically inserted lateral-wall cochlear-implant electrode arrays reduces forces on the basilar membrane in vitro', Otol. Neurotol., vol. 42, no. 7, pp. 1022–1030, Aug. 2021.

[13] J. Granna, T. S. Rau, T.-D. Nguyen, T. Lenarz, O. Majdani, and J. Burgner-Kahrs, 'Toward automated cochlear implant insertion using tubular manipulators', in Medical Imaging 2016: Image-Guided Procedures, Robotic Interventions, and Modeling, San Diego, California, United States, 2016.

[14] K. S. Min, S. B. Jun, Y. S. Lim, S.-I. Park, and S. J. Kim, 'Modiolus-hugging intracochlear electrode array with shape memory alloy', Comput. Math. Methods Med., vol. 2013, p. 250915, May 2013.

[15] R. Hagemann et al., 'Design, processing, and characterization of nickel titanium micro-actuators for medical implants', J. Laser Appl., vol. 27, no. S2, p. S29203, Feb. 2015.

[16] L. Zentner, S. Griebel, and S. Hügl, 'Fluid-mechanical compliant actuator for the insertion of a cochlear implant electrode carrier', Mech. Mach. Theory, vol. 142, no. 103590, p. 103590, Dec. 2019.

[17] R. J. S. Briggs et al., 'Development and evaluation of the modiolar research array - multi-centre collaborative study in human temporal bones', Cochlear Implants Int., vol. 12, no. 3, pp. 129-139, 2011.

[18] H. Rask-andersen and E. Erixon, 'Human Cochlea : Anatomical Characteristics and Their Relevance for Cochlear Implantation', no. March 2016, 2011.

[19] L. Leon, M. S. Cavilla, M. B. Doran, F. M. Warren, and J. J. Abbott, 'Scala-tympani phantom with cochleostomy and round-window openings for cochlear-implant insertion experiments', J. Med. Devices, Trans. ASME, vol. 8, no. 4, pp. 1-10, 2014.

[20] J. R. Clark, L. Leon, F. M. Warren, and J. J. Abbott, 'Investigation of magnetic guidance of cochlear implants', 2011 IEEE/RSJ Int. Conf. Intell. Robot. Syst., pp. 1321-1326, Dec. 2011.

[21] E. Boyer, A. Karkas, A. Attye, V. Lefournier, B. Escude, and S. Schmerber, 'Scalar localization by cone-beamcomputed tomography of cochlear implant carriers: A comparative study between straight and periomodiolar precurved electrode arrays', Otol. Neurotol., vol. 36, no. 3, pp. 422-429, 2015.

[22] N. R. Sinatra, T. Ranzani, J. J. Vlassak, K. K. Parker, and R. J. Wood, 'Nanofiber-reinforced soft fluidic micro-actuators', J. Micromechanics Microengineering, vol. 28, no. 8, p. aab373, 2018.